Plasmonic sectoral horn nanoantennas

Yuanqing Yang,[1] Ding Zhao,[1] Hanmo Gong,[1] Qiang Li,[1] and Min Qiu[1,2,*]

[1]*State Key Laboratory of Modern Optical Instrumentation, Department of Optical Engineering, Zhejiang University, Hangzhou 310027, China*

[2]*School of Information and Communication Technology, Royal Institute of Technology (KTH), Electrum 229, 164 40 Kista, Sweden*

**Corresponding author: minqiu@zju.edu.cn*

Received March 25, 2014; revised April 22, 2014; accepted April 22, 2014; posted April 23, 2014 (Doc. ID 208856); published May 23, 2014

In this Letter, plasmonic sectoral horn nanoantennas working at near-infrared wavelength (1550 nm) have been investigated. We demonstrate that, although there are certain differences between the plasmonic and classical radio-frequency (RF) sectoral horn antennas, the plasmonic horns still possess a number of attractive features, like their RF counterparts, such as tunable high directivities, simplicity in fabrication, and ease of coupling to waveguides. As a specific application, we further show how to exploit these findings to optimize an optical wireless nanolink using the proposed horn nanoantennas, and obtain a 60-fold increase in the received power compared with the situation of matched dipole nanoantennas.

OCIS codes: (250.5403) Plasmonics; (240.6680) Surface plasmons; (250.5300) Photonic integrated circuits.
http://dx.doi.org/10.1364/OL.39.003204

During the past few years, optical nanoantennas have attracted extensive attention because of their applications in a variety of fields, including near-field spectroscopy [1], photovoltaics [2], photodetection [3], light emission [4,5], sensing [6], nonlinear optics [7], and optical wireless communication [8–10]. Similar to their radiofrequency (RF) counterparts, optical nanoantennas could enable an efficient conversion between highly localized and propagating far-field electromagnetic waves [11]. Nevertheless, due to the fact that metals are no longer perfect conductors and support surface plasmon polaritons (SPPs) in optical regime, the design rules of RF antennas cannot be directly applied to optical nanoantennas [12]. Thus, pursing the RF antenna analogy is still a challenge and the subject of many recent scientific studies. A number of established RF antenna configurations and design methodologies have been successfully downscaled and adapted into the optical domain. These include monopole, half-wave dipole, bow-tie, cross, patch, and Yagi–Uda antennas [10–17].

Despite lots of work to develop the optical analogy of RF antennas, little research on horn nanoantennas has been conducted, given their widespread use in the RF region [18–20]. A horn antenna can be regarded as a waveguide flared to a larger opening, which can produce a uniform phase front and, hence, increase the directivity. Therefore, for a horn antenna, the radiating element and the waveguide are inherently coupled. In this context, Ramaccia *et al.* first proposed an efficient and wideband horn nanoantenna using a gradual exponential taper with dozens of cylindrical silver pillars [18]. However, to establish a design methodology for the plasmonic horn antenna, there is still a serious lack of effort in studying the behavior of the horn nanoantennas systemically.

In this Letter, we present a thorough study in the behavior of the sectoral horn nanoantennas with straight flares. The results demonstrate that, although there are certain differences between the plasmonic and RF sectoral horn antennas, the plasmonic horns still possess advantages, such as ease of excitation and tunable high directivities, just like their RF counterparts. Moreover, the proposed plasmonic horns also owe their advantages to ease of fabrication and integration and are easily prepared by FIB (focused ion beam) or EBL (E-beam lithography) techniques. Finally, as a specific application, by applying our previous findings, we optimize an optical wireless nanolink using the proposed horn nanoantenna and achieve a 60-fold increase in the received power compared with the situation using matched dipole nanoantennas.

The nanostructure is modeled and simulated by the finite-difference time-domain (FDTD) method (FDTD Solutions, version 8.6.4). We assume a wavelength λ_0 of 1550 nm in the vacuum and the whole sectoral horn nanoantenna fully embedded in the glass ($n = 1.44$) contains a piece of two-wire optical transmission line (OTL), with a flare in only one dimension (along z axis), as illustrated in Fig. 1. The OTL consists of two silver ($\varepsilon = -130.80 + 3.32j$) [21] parallel wires (the length is a) with rectangular cross sections ($b \times c$ nm^2), separated by a glass gap g. In the following calculations, since we are more concerned with the properties and influences of the opening flare, here the geometric parameters of the OTLs a, b, c, g are fixed to 1000, 100, 50, and 30 nm, respectively. The length and the flaring angle of the tapered opening are l and θ while t represents the width of the silver wire at the end of the horn. To feed the plasmonic horn nanoantenna, we first calculate the fundamental mode supported by the OTL using an integrated mode

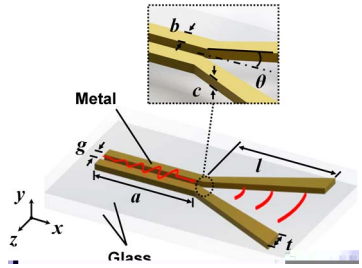

Fig. 1. Schematic of the plasmonic sectoral horn nanoantennas.

analysis in FDTD Solutions, and then exploit it as the light source to excite the OTL. This approach will make sure the guided wave propagating in the OTL is only the fundamental mode (with E-field in z direction) and has been successfully excited and obtained.

To reveal the performance of the plasmonic sectoral horn nanoantenna, a typical 2D near-field electric intensity map and its corresponding far-field directivity patterns (linear scale, similarly hereinafter) are drawn in Fig. 2 with a set of parameters l, θ, and t being 1000 nm, 26.6°, and 100 nm, respectively. The directivity D of the nanoantenna is defined as [12]:

$$D(\theta,\phi) = \frac{4\pi}{P_{\text{rad}}} p(\theta,\phi), \tag{1}$$

where θ, ϕ represent the observation angles while P_{rad} and $p(\theta,\phi)$ are the total radiated and angular power densities, respectively. In Fig. 2(a), the near-field electric intensity image shows that the flare provides a gradual increase in the physical aperture and a progressive impedance matching between the OTL and free-space. A relatively uniform E-field distribution outside the aperture of the horn can be clearly seen, indicating a high directivity is attained. A high maximum directivity (~13.85) can be obtained on the x axis that coincides with the propagation direction. Moreover, for the proposed sectoral horn nanoantenna, the opening is only flared in the direction of the E-field. For this reason, the main lobe of the E-plane pattern (XZ plane) is much narrower than the H-plane (XY plane), just like its RF counterpart [20], as depicted in Fig. 2(b).

Since the directivity of an antenna represents its ability to direct the far-field radiation and improve the intensity concentration in a desired direction [20], it is a significant parameter to describe the far-field properties of the antenna. Therefore, we further examine the directivity D of the horn nanoantenna as a function of the variation in the geometric parameters. Directivity patterns of horn nanoantennas, with fixed θ(26.6°) and t(100 nm), and different lengths l, are plotted in Fig. 3. As the length increases, the directivity increases as well, and the beam width of the radiation pattern becomes narrower. The maximum directivity is attained with the side lobes, almost vanishing when $l = 1000$ nm. However, when the length continues to increase, a radiation pattern with a reduced directivity is obtained, as sketched in Fig. 3(d). A similar trend can be seen when the flare angle θ of the horn nanoantenna varies while the length l and the width t are held constant

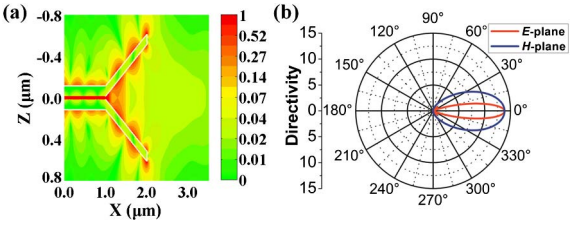

Fig. 2. (a) 2D map of near-field electric intensity recorded in the XZ plane ($y = 25$ nm) of the horn nanoantenna with $l = 1000$ nm, $\theta = 26.6°$, and $t = 100$ nm. (b) Corresponding directivity pattern (linear scale, similarly hereinafter) of the plasmonic sectoral horn. nanoantennas.

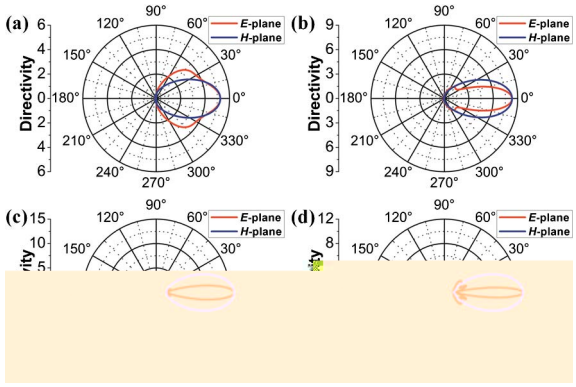

Fig. 3. Directivity patterns of plasmonic sectoral horn nanoantennas with constant θ(26.6°) and t(100 nm) as a function of different lengths, including (a) $l = 100$ nm, (b) $l = 500$ nm, (c) $l = 1000$ nm, and (d) $l = 1500$ nm.

($l = 1000$ nm, $t = 100$ nm), as illustrated in Fig. 4. For small included angles, the side lobes gradually diminish and the pattern becomes narrower as the flare increases. Beyond a certain angle, the directivity then starts to decrease and the minor lobes appear again. Furthermore, given the proposed plasmonic horns are nonresonant, they also possess broadband behaviors. For the same set of geometric parameters as in Fig. 2, the plasmonic horn nanoantenna exhibits a directivity higher than 10 in a broadband region over 650 nm. The change in the bandwidth also follows the same trend of the radiation pattern. It should be pointed out that these noticeable relations between the radiation characteristic and the geometric parameters are in like manner with the RF E-plane sectoral horns [20,22].

At the same time, attention should also be paid to the differences between the plasmonic and classical RF horn antennas. For the RF horn antennas, an approximation to neglect the fields outside the aperture is usually done. The thickness of the metal at the aperture of the horn hence has no influence in the radiation properties. However, as shown in Fig. 5, when the width t of the silver OTL at the end of the horn nanoantennas is varied, the radiation properties change as well. For the situations that the width t is relatively small compared to the aperture, the variations in the width t have only

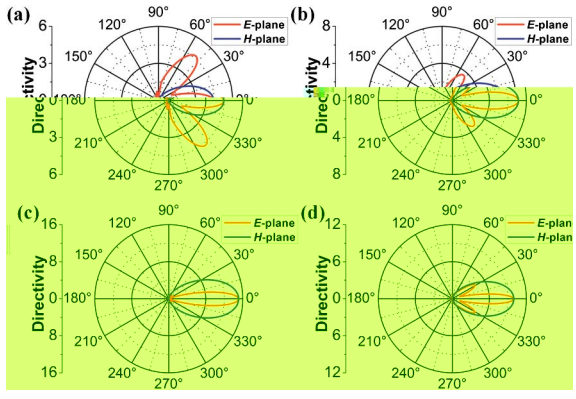

Fig. 4. Directivity patterns of plasmonic sectoral horn nanoantennas with constant l(1000 nm) and t(100 nm) as a function of different flare angles, including (a) $\theta = 7.7°$, (b) $\theta = 13.2°$, (c) $\theta = 30.3°$, and (d) $\theta = 38.1°$.

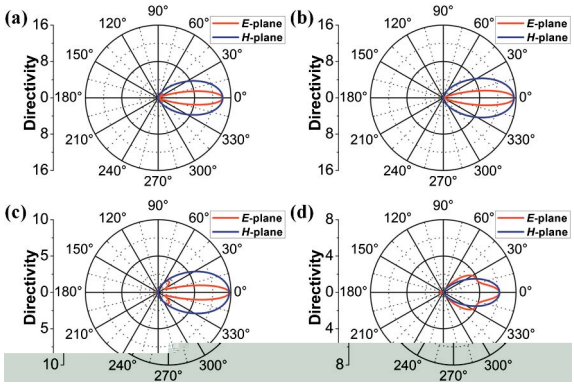

Fig. 5. Directivity patterns of plasmonic sectoral horn nanoantennas with constant l(1000 nm) and θ(26.6°) as a function of different widths, including (a) $t = 50$ nm, (b) $t = 200$ nm, (c) $t = 400$ nm, and (d) $t = 600$ nm.

a slight impact on the radiation properties, as Figs. 5(a)–5(c) present. Nevertheless, as depicted in Fig. 5(d), if the width continues to increase, then the directivities will decrease remarkably. This is mainly due to the fact that the penetration of the electromagnetic waves into silver is non-negligible at optical frequencies. Therefore, fields outside the aperture of the plasmonic horn nanoantennas can no longer be assumed to be zero. The width t of silver may lead to variations in the magnitude and phase of the field across the aperture, resulting in the changes of the directivity. Figure 6 depicts the E-field distributions over the aperture of the horn nanoantennas with different widths t. When $t = 200$ nm, the E-fields in the ends of the horn are similar to the long-range surface plasmon (SP) mode with mirror symmetry with respect to the gap [23]. The electric fields are mainly concentrated on the outer surface of the metal strips. Thus, in this situation, the whole flaring-out plasmonic horn changes a highly confined mode inside the OTL to a nonradiative long-range mode. The E-field in the proximity of the metal, therefore, has a slight impact on the far-field radiation, as the RF horn antennas do. However, when $t = 600$ nm, the E-field in the ends of the horn are similar to two weakly coupled dipole-like oscillations. As a consequence, its near-field distribution breaks the uniform phase over the aperture of the horn and its contribution to the far-field radiation would decrease the directivity.

Although there exist certain differences between the plasmonic and RF horns, the aforementioned result

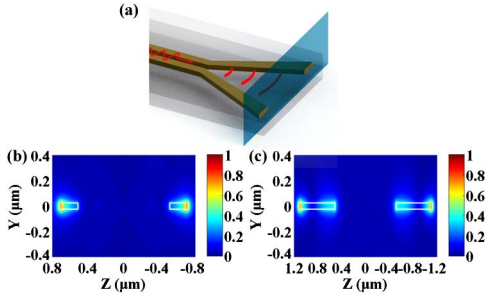

Fig. 6. E-field distributions over the aperture of the horn nanoantennas (a) with different widths t (b) $t = 200$ nm, and (c) $t = 600$ nm.

demonstrate that plasmonic sectoral horn nanoantennas can still be easily fed by the waveguides and possess tunable high directivities. These exciting features may open a new door for extensive applications. In particular, optical wireless communication based on plasmonic nanoantennas has been recently proposed and attracted wide interest, as an integral part of nanoscale optical circuits for future chip-scale data processing and computations [8–10].

Thus, in the following, we show how to exploit our findings to use the proposed horn nanoantennas to build a point-to-point optical wireless nanolink. The overall performance of such a communication system is judged by the Friis Transmission Equation [20]:

$$\frac{P_r}{P_t} = e_t e_r D_t D_r |\mathbf{p_t} \bullet \mathbf{p_r}|^2 \left(\frac{\lambda_0}{4\pi n d}\right)^2, \tag{2}$$

where P_r and P_t are the received and transmitted power of the communication system, e_t and e_r are the total efficiency of the transmitting and receiving terminals, D_t and D_r are the directivities of the transmitting and receiving antennas, $|\mathbf{p_t} \bullet \mathbf{p_r}|^2$ represents the polarization mismatch and the term $((\lambda_0/4\pi nd)^2$ is called the free-space loss factor, which is related to the operating wavelength λ_0 in vacuum, the environmental refractive index n, and the distance d between the transmitting and receiving terminals. The total efficiency e_t is defined as the ratio of the far-field radiated power P_{rad} and the input power P_{in} to the terminal. Here, we first determine the input power P_{in} by using a perfectly matched layer (PML) to terminate the OTL and then integrate the Poynting vector over the interface between the OTL and the PML. Then, we substitute the flared opening for the PML and obtain the radiated power P_{rad} by integrating the Poynting vector across a closed surface that contains the horn. For simplicity, we apply the same horn nanoantennas in both transmitting and receiving ends with matched polarization; then, we are only concerned with e_t and D_t because of the reciprocity theorem. We further introduce and define the quality factor Q of an optical wireless nanolink as $Q = e_t D_t e_r D_r$. Therefore, to obtain the best overall performance of the nanolink, we need to increase the Q as high as possible.

A set of optimized parameters is given as $l = 1000$ nm, $\theta = 18.6°$ and $t = 320$ nm. Figure 7(a) shows the electric field distribution in a complete point-to-point optical wireless nanolink. The distances d between the transmitting and receiving terminals are 3 μm. It can be clearly seen that, with the proper design, the transmitting terminal successfully converts localized energy inside the OTL into far-field radiations with a relatively uniform distribution. After travelling in free-space for a distance d, the energy is collected by the receiving end and coupled into the propagating mode supported by the OTL. Figure 7(b) describes the far-field properties of the optimized horn nanoantenna. Most of the radiation is focused on the propagation direction, with no minor lobes shown in E-plane. Figure 7(c) demonstrates that a highly confined mode is excited and propagated inside the OTL in the receiving end. The optimized Q is as high as 32.24, with the directivity D_t of 13.18, and the total efficiency e_t of

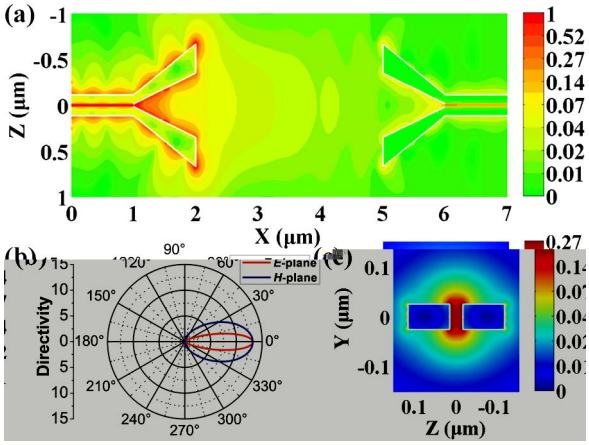

Fig. 7. (a) E-field intensity distribution recorded in the XZ plane ($y = 25$ nm) of the optimized horn nanoantenna ($l = 1000$ nm, $\theta = 18.6°$, and $t = 320$ nm). (b) Directivity pattern of the optimized horn nanoantenna used in the optical wireless nanolink. (c) E-field distribution inside the OTL of the receiving terminal.

43.08%. Then, we can calculate the ratio between P_t and P_r based on the Friis Transmission Equation and the result is 0.0263 (−15.80 dB), which is in good agreement with the result obtained from the FDTD simulation (−15.88 dB). Here, it should be noted that the Friis equation is valid not only for the far-field, but also for the region close to the border between the near- and far-fields (e.g., a distance of 3 μm in our situation). As a reference, when we also calculate the optical wireless nanolink using matched dipole nanoantennas at near-infrared region according to the previous report [9], an optimized quality factor Q of 0.52 can be attained, with the directivity D_t near 1.5 and the total efficiency e_t of 48.09%. Therefore, an optical wireless nanolink using the proposed sectoral horn nanoantennas show a 60-fold increase in the ratio of the received power P_r to the transmitted power P_t. Additionally, we also want to stress that it is due to the significant absorption loss in the metal at optical frequencies that the plasmonic horn nanoantennas own relatively low efficiencies compared with the RF horns, whose efficiencies are near to unity.

In summary, plasmonic sectoral horn nanoantennas with straight flares have been investigated. We study the relations between the far-field radiation properties of the horn nanoantennas and their geometric parameters. Theoretical results demonstrate that, despite certain differences between the plasmonic and classical RF horn antennas, the sectoral nanoantennas in optical regime still own a variety of attractive features, such as tunable high directivities and inherent coupling between the radiating elements and the feeding waveguides, which offer new possibilities for many exciting applications. In particular, we build an optical wireless communication link using the proposed horn nanoantennas. A 60-fold increase in the received power is obtained compared with the situation using matched dipole nanoantennas. Furthermore, from the experimental point of view, the presented sectoral horn nanoantennas with straight flares is basically a metal–insulator–metal waveguide with a tapered-out opening, which could be easily prepared and fabricated by FIB or EBL techniques. We expect that such a systematical study of the proposed horn nanoantennas will inspire future experimental works and may pave the way for pursing the optical analogy of RF antennas.

This work is supported by the National Natural Science Foundation of China (Grant Nos. 61275030, 61205030, and 61235007), Qianjiang River Fellow Fund of Zhejiang Province, the Scientific Research Foundation for the Returned Overseas Chinese Scholars from the State Education Ministry, the Opened Fund of State Key Laboratory of Advanced Optical Communication Systems and Networks, the Fundamental Research Funds for the Central Universities (2014QNA5020), Doctoral Fund of Ministry of Education of China (Grant No. 20120101120128) and the Swedish Research Council (VR).

References

1. P. Bharadwaj, R. Beams, and L. Novotny, Chem. Eng. Sci. **2**, 136 (2011).
2. H. A. Atwater and A. Polman, Nat. Mater. **9**, 205 (2010).
3. M. W. Knight, H. Sobhani, P. Nordlander, and N. J. Halas, Science **332**, 702 (2011).
4. A. G. Curto, G. Volpe, T. H. Taminiau, M. P. Kreuzer, R. Quidant, and N. F. van Hulst, Science **329**, 930 (2010).
5. K. G. Lee, X. W. Chen, H. Eghlidi, P. Kukura, R. Lettow, A. Renn, and V. S. S. Götzinger, Nat. Photonics **5**, 166 (2011).
6. J. N. Anker, W. P. Hall, O. Lyandres, N. C. Shah, J. Zhao, and R. P. Van Duyne, Nat. Mater. **7**, 442 (2008).
7. M. Kauranen and A. V. Zayats, Nat. Photonics **6**, 737 (2012).
8. J.-S. Huang, T. Feichtner, P. Biagioni, and B. Hecht, Nano Lett. **9**, 1897 (2009).
9. A. Alù and N. Engheta, Phys. Rev. Lett. **104**, 213902 (2010).
10. D. M. Solís, J. M. Taboada, F. Obelleiro, and L. Landesa, Opt. Express **21**, 2369 (2013).
11. P. Bharadwaj, B. Deutsch, and L. Novotny, Adv. Opt. Photon. **1**, 438 (2009).
12. L. Novotny and N. F. van Hulst, Nat. Photonics **5**, 83 (2011).
13. R. Adato, A. A. Yanik, and H. Altug, Nano Lett. **11**, 5219 (2011).
14. P. Mühlschlegel, H. J. Eisler, O. J. F. Martin, B. Hecht, and D. W. Pohl, Science **308**, 1607 (2005).
15. P. Biagioni, J. S. Huang, L. Duò, M. Finazzi, and B. Hecht, Phys. Rev. Lett. **102**, 256801 (2009).
16. R. Esteban, T. V. Teperik, and J. J. Greffet, Phys. Rev. Lett. **104**, 26802 (2010).
17. H. Zhao, Y. Yang, Q. Li, and M. Qiu, Appl. Phys. Lett. **103**, 261108 (2013).
18. D. Ramaccia, F. Bilotti, A. Toscano, and A. Massaro, Opt. Lett. **36**, 1743 (2011).
19. T. Grosjean, M. Mivelle, G. W. Burr, and F. I. Baida, Opt. Express **21**, 1762 (2013).
20. C. A. Balanis, *Antenna Theory: Analysis and Design* (Wiley, 2005).
21. P. B. Johnson and R. W. Christy, Phys. Rev. B **6**, 4370 (1972).
22. D. R. Rhodes, Proc. IRE **36**, 1101 (1948).
23. G. Veronis and S. Fan, J. Lightwave Technol. **25**, 2511 (2007).